UDC 621.3 https://doi.org/10.20998/2074-272X.2025.4.05

Z. Khammassi, H. Khaterchi, A. Zaafouri

Experimental analysis of the effects of potential-induced degradation on photovoltaic module performance parameters

Introduction. *Photovoltaic (PV) power plants are subject to various forms of degradation that can impair their performance and lead to significant faults within PV systems. Among these, Potential-Induced Degradation (PID) stands out as one of the most severe, impacting the efficiency and output of PV generators while shortening their lifespan.* ***Problem****. This phenomenon is the result of a decrease in the shunt resistance of the cells encapsulated within the PV module, directly associated with a reduction in its insulation resistance. Although extensive research has been conducted in this area, our understanding of the factors contributing to PID, as well as its detection and effects on PV systems, remains incomplete. The* ***goal*** *of this work is to investigate the variations in insulation resistance at the module's glass and frame, and to map the changes in shunt resistance at the module level to identify the most vulnerable areas, characterized by lower insulation resistance values and significantly affected by PID.* ***Methodology.*** *This study utilizes a comparative experimental method to investigate the behavior of two identical PV modules under similar climatic conditions, where one module is exposed to voltage stress while the other remains unstressed. A high-voltage insulation resistance tester was employed to apply voltage stress between the terminals of the stressed module and its metal frame, with insulation resistance systematically measured at various points to analyze changes in electrical properties. The* ***originality*** *of this study lies in the estimation of the shunt resistance based on the operating voltage of the PV string, which depends on the types of grounding, climatic conditions such as temperature and humidity, as well as the position of the cell within the PV module. This estimation is correlated with the I-V characteristic curves of two PV modules, one of which is subjected to operating voltages under well-controlled environmental conditions. The* ***results*** *reveal that an increase in the test voltage leads to a reduction in insulation resistance, a phenomenon that becomes more pronounced in humid environments. This highlights the vulnerability of PV modules to PID, which can significantly affect their lifespan and performance, particularly through the reduction of shunt resistance and the distortion of the characteristic curve of the stressed module affected by this phenomenon, thereby causing increased difficulty in extracting its maximum power.* References 30, table 3, figures 17.
Key words: **potential-induced degradation, insulation resistance, maximum power point tracking, solar photovoltaic system.**

Вступ*. Фотоелектричні (PV) електростанції схильні до різних форм деградації, які можуть погіршити їхню продуктивність і призвести до значних несправностей у PV системах. Серед них потенціально-індукована деградація (PID), виділяється як одна з найсерйозніших, впливаючи на ефективність та вихідну потужність PV генераторів, одночасно скорочуючи термін їхньої служби.* ***Проблема****. Це явище є результатом зниження опору шунтуючого з'єднання елементів, вбудованих у PV модулі, що безпосередньо пов'язано зі зниженням опору його ізоляції. Хоча в цій галузі було проведено широкі дослідження, наше розуміння факторів, що сприяють PID, а також його виявлення та впливу на PV системи, залишається неповним.* ***Метою*** *роботи є дослідження змін опору ізоляції на склі та каркасі модуля, а також картографування змін опору шунтуючого з'єднання на рівні модуля для виявлення найбільш вразливих зон, що характеризуються нижчими значеннями опору ізоляції та значно зазнають впливу PID.* ***Методологія****. У цьому дослідженні використовується порівняльний експериментальний метод для дослідження поведінки двох ідентичних PV модулів за подібних кліматичних умов, де один модуль піддається впливу напруги, а інший залишається ненапруженим. Для застосування напруги між клемами напруженого модуля та його металевим каркасом було використано високовольтний тестер опору ізоляції, при цьому опір ізоляції систематично вимірювався в різних точках для аналізу змін електричних властивостей.* ***Оригінальність*** *дослідження полягає в оцінці опору шунту на основі робочої напруги PV кола, яка залежить від типів заземлення, кліматичних умов, таких як температура та вологість, а також положення елемента всередині PV модуля. Ця оцінка корелює з ВАХ двох PV модулів, один з яких піддається робочій напрузі в добре контрольованих умовах навколишнього середовища.* ***Результати*** *показують, що збільшення випробувальної напруги призводить до зниження опору ізоляції, явище, яке стає більш вираженим у вологому середовищі. Це підкреслює вразливість PV модулів до PID, що може суттєво вплинути на їхній термін служби та продуктивність, зокрема через зменшення опору шунту та спотворення характеристик модуля, що піддається впливу цього явища, що призводить до збільшення труднощів в отриманні його максимальної потужності.* Бібл. 30, табл. 3, рис. 17.
Ключові слова: **потенціально-індукована деградація, опір ізоляції, відстеження точки максимальної потужності, сонячна фотоелектрична система.**

Introduction. The contemporary energy and environmental landscape is defined by a significant demand for primary energy sources. Despite the growth of renewable energy, fossil fuels continue to dominate the global energy mix [1, 2]. The International Energy Agency estimates that global energy demand could rise by 45 % by 2030 due to population growth and industrialization in developing nations. This increase would lead to higher carbon dioxide (CO_2) emissions, the primary greenhouse gas produced by fossil fuel combustion, which significantly contributes to global warming and climate change, impacting agriculture and water resources [3–5]. To address these challenges, humanity must explore sustainable, renewable, and cost-effective energy alternatives. Renewable energy systems such as solar, photovoltaic (PV), wind, hydropower, biomass and geothermal energy represent promising options. Among these, PV energy stands out as a sustainable and economically viable technology. Over the past decade, global PV installations have surged from 229 GW in 2015 to 1,177 GW by the end of 2022. That year alone, 239 GW of solar capacity was added, marking a 45 % increase compared to 2021. If this trend persists, global PV capacity could reach 800 GW by 2027 and 1 TW by 2030 [6]. The work [7] analyzes the effects of aging on PV modules, showing an annual power loss of 1 % and a resistance increase of 12.8 % over 20 years, impacting large-scale systems. The article [8] examined the effect of aging PV modules on the electrical

performance of grid-connected systems, revealing a 1 % annual reduction in maximum power and a 12.8 % increase in resistance over 20 years. Projections indicate a cumulative capacity of approximately 4.7 TW, accounting for 16 % of the global electricity mix by 2050. This rapid expansion has enhanced attention on PV technology reliability, considering factors such as system configurations, module size, technology, climatic zones, and degradation mechanisms like microcracks, discoloration, hot spots, glass breakage, corrosion, and specific forms of degradation such as ultraviolet light-induced degradation, light-induced degradation, moisture-induced degradation, and Potential-Induced Degradation (PID) [9–12]. The reliability of PV modules is affected by degradation mechanisms such as PID, which significantly reduces power output, especially in rooftop installations and hot climates, and although difficult to detect through annual production data, it was clearly identified by infrared imaging and linked to a linear decrease in the performance of a 314 kWp plant [13]. Diagnostic advancements include real-time thermoelectrical models linking degradation to environmental factors [14], modified Maximum Power Point Tracking (MPPT) techniques for defect detection [15], and artificial intelligence tools enabling rapid and accurate fault diagnosis in under 9 s [16]. Studies highlight PID's substantial impact on mono- and multi-crystalline modules, with power losses of up to 18.7 % after 96 hours of stress [17], and explore its mechanisms, evaluation methods, mitigation strategies, and recovery under environmental influences [18]. The works [19–21] examine common defects in PV modules, including cell cracks and hot spots. These insights aid in improving module durability and performance monitoring. Among these, PID has been observed in all PV technologies and in almost all operating climates. It does not occur so frequently, but if it does it effect can lead to a severe performance loss within a short period PID identified as a major contributor to higher degradation rates, particularly in younger modules. With the accelerated deployment of large-scale PV plants, designers aim to boost profits while keeping investment and operational costs low. To achieve this, they increase the voltage across PV strings by connecting more modules in series. This approach reduces ohmic losses in wiring and lowers installation and operational costs by decreasing the number of cables, connectors, junction boxes, and inverters required. Consequently, PV module voltage levels have evolved from 600 V in 1990 to 1 kV in 2010, with the current industry standard being 1.5 kV. Research is ongoing to explore even higher voltage levels. Discovered in 2010, PID has been extensively studied to understand its underlying mechanisms and develop mitigation strategies. Its significance has grown in recent years due to its potential to cause severe module failures under certain conditions [22, 23]. The paper [24] studied the recombination behavior of solar modules affected by PID, and based on the findings, analyzed the relative mismatch losses of these PID-affected modules. The mismatch effect, resulting from partial shading, is highlighted in [25]. The phenomenon generated impacts the maximum power extraction technique mentioned in [26]. PID results from a high potential difference between PV cells and the module frame, particularly at the ends of PV strings in grid-connected systems. This potential difference can cause leakage currents, leading to performance degradation [27]. The trend toward higher system voltages (up to 1.5 kV) exacerbates this issue. PV systems, which consist primarily of PV strings and inverters, are characterized by electrical parameters such as open-circuit voltage (V_{oc}), short-circuit current (I_{sc}), DC voltage connecting each string to the MPPT input of the inverter, and AC voltage output from the inverter. The work [28] presents an innovative IoT-based system for fault detection in hybrid PV installations, aimed at improving reliability, grid stability, and fault management through advanced algorithms. The paper [29] proposes an optimized sensor placement model, validated through simulations, enabling precise fault detection and enhancing system reliability and maintenance. Finally, the work [30] develops a fuzzy logic-based algorithm to detect and classify 12 types of faults in PV systems, ensuring optimal energy production and improved reliability.

The goal of this work is to investigate the variations in insulation resistance at the module's glass and frame, and to map the changes in shunt resistance at the module level to identify the most vulnerable areas, characterized by lower insulation resistance values and significantly affected by PID.

This study focuses on a comparative experimental analysis conducted on two identical PV modules exposed to the same climatic conditions. A high-voltage insulation resistance tester was employed to apply a voltage stress between the terminals of one module and its metal frame while measuring the insulation resistance at various points. Subsequently, the *I-V* curves of both modules were plotted under similar climatic conditions. The objective is to examine the variation in insulation resistance at the module's glass and frame, identified as a critical factor contributing to PID.

Methods. Modeling of PV string elements. In a grid-connected PV system, inverters are designed to accommodate various input voltage ranges, typically up to 600 V, 1 kV, or even 1.5 kV, depending on standards and design specifications. This flexibility enables the maximization of power generated by PV modules. To meet these operational requirements, multiple modules are connected in series to form a PV string, ensuring that the voltage at its terminals aligns with the inverter's input range.

PV cell is the smallest component of a PV string, designed to capture irradiation and convert it into electricity through the PV effect. It serves as the core element of the PV conversion process and can be likened to a current source. When exposed to light, a PV cell generates a high current (typically ranging from 6 A to 8 A) compared to its relatively low voltage (0.4 V to 0.6 V), which results in a limited power output. Therefore, it is essential to connect multiple cells in series or parallel configurations to produce a usable power level.

We adopted a five-parameter model of PV cell. It consists of a photocurrent source (I_{ph}) generated by irradiation, placed in parallel with a diode D and a parallel resistance R_{sh}, which represents the path for leakage current at the edge of the cell, caused by impurities, electron-hole recombination, irregularities in the N-P junction thickness, and the presence of cracks in the cell. Additionally, a series resistance R_s is connected in series with these components, representing ohmic losses in the collectors, fingers, the contact resistance between the metal and semiconductor, as

well as the interconnections between PV cells (Fig. 1). The photocurrent I_{ph} generated by a single PV cell is directly proportional to the incident irradiance (G, W/m²) and dependent on the temperature (T, K).

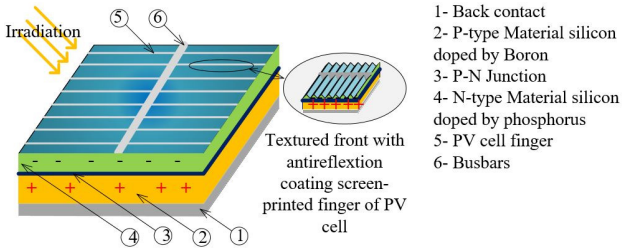

Fig. 1. PV cell

In accordance with the equivalent scheme of a PV cell (Fig. 2), and applying Kirchhoff's law, the current-voltage characteristic equation of a PV cell is:

$$I = I_{ph} - I_d - I_{sh}, \quad (1)$$

where I is the output current; I_{ph} is the photocurrent. Equations (2), (3) also define the diode current I_d and the shunt resistor current I_{sh}

$$I_d = I_{sd}\left[\exp\left(\frac{V + R_s I}{A V_t}\right) - 1\right]; \quad (2)$$

$$I_{sh} = \frac{V + R_s I}{R_{sh}}; \quad (3)$$

$$V_t = kT/q; \quad (4)$$

$$I = I_{ph} - I_{sd}\left[\exp\left(\frac{V + R_s I}{A V_t}\right) - 1\right] - \frac{V + R_s I}{R_{sh}}, \quad (5)$$

where R_s is the series resistance; A is the diode ideality factor (typically ranging from 1 to 2); R_{sh} is the shunt resistance; V_t is the thermal voltage of the diode; k is the Boltzmann constant; q is the electron charge; T is the cell temperature.

The saturation current I_{sd} is influenced by temperature, the surface area of the diode (and thus the PV cell), and the properties of the junction. It varies exponentially with temperature and can be represented as:

$$I_{sd} = I_{sc}\left(\frac{T_{op}}{T_{ref}}\right)^3 \exp\left(\frac{qE_g}{Ak}\left(\frac{1}{T_{ref}} - \frac{1}{T_{op}}\right)\right); \quad (6)$$

$$I_{ph} = I_{sc} + k_i\left(T_{op} - T_{ref}\right)\frac{G}{G_0}, \quad (7)$$

where I_{sc} is the short-circuit current of the PV cell; T_{op} is the operating temperature of the PV cell; T_{ref} is the reference temperature of the PV cell; E_g is the optical band gap of the material; k_i is the temperature coefficient at short-circuit; G_0 is the irradiance under standard test conditions; G is the irradiance under the operating conditions.

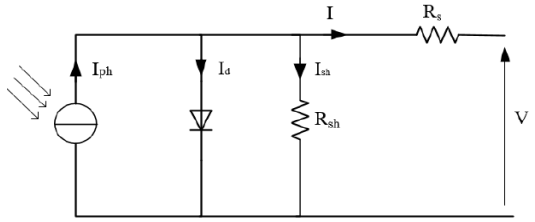

Fig. 2. Equivalent scheme of a PV cell

PV module is a device designed to capture sunlight and convert it into electricity through the PV effect. It is an essential component in PV systems. The module is made up of several identical PV cells connected in series or parallel to achieve specific required characteristics such as voltage, current, and fill factor. To obtain a usable voltage across the terminals of a PV module, the cells that constitute it must be connected in series to increase the voltage at the terminals and reduce ohmic losses. However, with this configuration of cells, in the case of partial or total shading of a cell, the current generated by that cell will decrease, leading to a reverse voltage across its terminals. This causes a local temperature increase and generates the phenomenon of hot spots, which can result in cell failures and module malfunction. Therefore, adding bypass diodes is crucial to limit this effect also to minimize the effect of shading on PV modules and reduce ohmic losses, a half-cell technology has been developed and commercialized. This technology is based on the parallel connection of identical half-cell groups, which are connected in series. PV cells are only a part of the overall laminated structure. This structure also includes components such as the module packaging (protective glass, encapsulant, backsheet), internal circuitry (electrodes, interconnections), bypass diodes, junction boxes, frame, cables, and connectors. Each of these elements can affect the reliability of the PV module (Table 1).

Table 1

Example of characteristics of a PV module

Characteristics	Value
Maximum power P_{max}, W	165
Open-circuit voltage V_{oc}, V	23.45
Short-circuit current I_{sc}, A	8.8
Voltage at maximum power V_{mpp}, V	19.4
Current at maximum power I_{mpp}, A	8.51
Maximum system voltage, V	1000
Temperature coefficient for P_{max}, %	–0.45
Number of cells connected in series N_s	36
Type of cell	polycrystalline
Number of bypass diodes in the junction box	2
Diode quality factor	1.3
Series resistance R_s, Ω	0.15
Parallel resistance R_{sh}, Ω	120
Optical band gap of the material E_g, eV	1.1

PID in PV systems. Connecting multiple PV modules in series to achieve the required voltage range for the inverter results in high voltage within the PV string. The selection and proper grounding of the DC side are crucial for ensuring the stable operation of the electrical PV system. Furthermore, to guarantee safety, the metal frames of the PV modules must be grounded (Fig. 3).

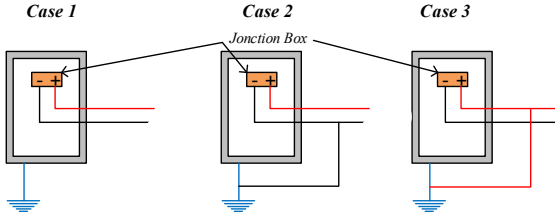

Fig. 3. Types of grounding for PV module frames

Depending on the type of inverter (with or without a transformer) and the selected grounding configuration, a significant voltage may develop between the module frames and the PV cells. This can lead to PID, which

shortens the system's lifespan and may cause operational failures. The following sections outline the various inverter configurations based on grounding topologies that are adapted for PV Generator.

A floating ground. Transformerless inverters do not offer galvanic isolation between the DC and AC sides, which may lead to specific potential differences within the system. When these inverters are used, a floating ground topology is often employed, as it is the most commonly used configuration, particularly in humid areas. This approach reduces the need for complex isolation systems and lowers the installation cost. The negative voltage generated across the PV string gradually induces the PID effect through the progressive accumulation of charges. This voltage draws electrical charges toward the surface of the PV cells, disrupting their operation and leading to a loss of efficiency. Over time, the PID effect degrades the performance of PV cells, reducing their electricity production capacity.

The maximum voltage responsible for this effect, as shown in Fig. 4, is given as:

$$V_{PID} = -\frac{1}{2} n_s V_{op}, \quad (8)$$

where n_s is the number of modules in a PV string; V_{op} is the operating voltage of a PV module; V_{PID} is the PID voltage.

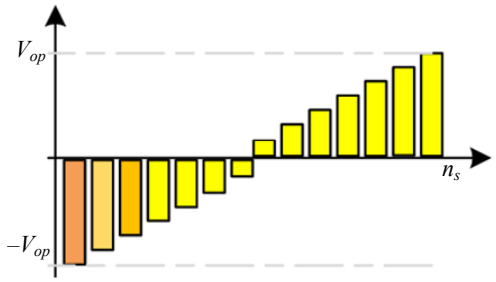

Fig. 4. Conversion with a transformerless inverter

Positive pole grounding. This topology is implemented with a transformer-based inverter that provides galvanic isolation between the DC and the AC sides. It is rarely used because it leads to a significant PID effect. This phenomenon results from the high negative voltage applied to the modules at the end of the string, this increases their susceptibility to PID, as illustrated by the negative voltage generated along the entire string, shown in Fig. 5,*a*, and represented as

$$V_{PID} = -n_s V_{op}. \quad (9)$$

Negative pole grounding. Installations located in dry or moderately humid environments favor this configuration (Fig. 5,*b*) due to the relatively low risk of corrosion compared to coastal or highly humid regions. This topology is implemented with a transformer-based inverter, providing galvanic isolation between the DC and the AC sides (Fig. 6). It ensures a positive voltage between the PV cells and the module frame, thus reducing the risk of degradation caused by PID. Furthermore, this configuration is particularly suitable for large-scale installations, as it helps extend the lifespan of the modules, although it may increase their vulnerability to corrosion.

The main cause of PID is the high voltage between the solar cells and the glass surface at the front of the module, as illustrated in the following figures.

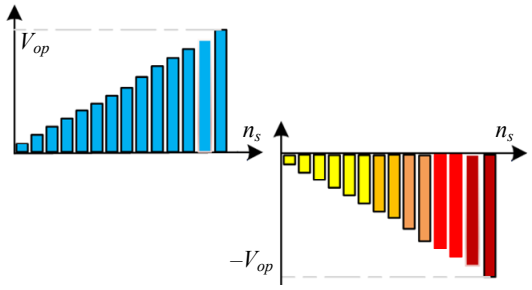

a) grounding the negative pole *b*) grounding the positive pole

Fig. 5. Conversion with transformer-based inverter

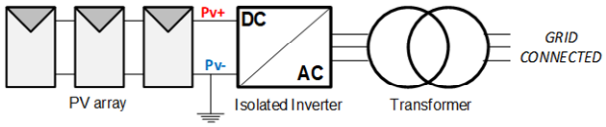

Fig. 6. Grounding topology for the negative pole of the PV string

PID affects the PV cell by increasing the leakage current. Leakage current refers to the current flowing from the base to the emitter without passing through the load (Fig. 7). This current can be categorized into 4 distinct types. First, the current may leak through the sodalime glass and the water molecules present on the surface (I_1). Second, current can leak due to electrons or ions on the upper surface of the cell (I_2). Third, leakage can occur through the ethylene-vinyl acetate (EVA) encapsulation layer (I_3). Finally, current can leak through the rear contact, thus completing the circuit (I_4).

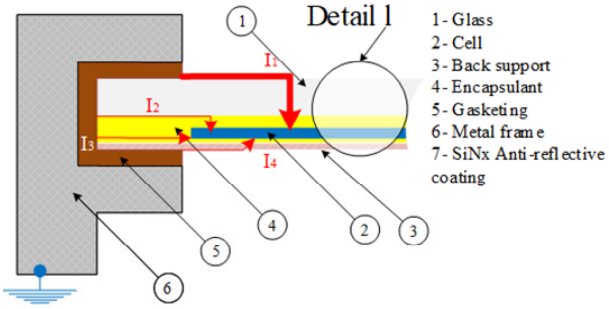

Fig. 7. Leakage current caused by the PID effect

To clearly explain PID at the cell and module levels, a voltage divider circuit is used. It is hypothesized that the intensity of the electric field in the SiNx layer plays a key role in the development of PID (Fig. 8,*a*). Three resistances, representing each layer, are connected in series to model the main path of the leakage current (glass, encapsulation sheet, and SiNx anti-reflection coating on the solar cell).

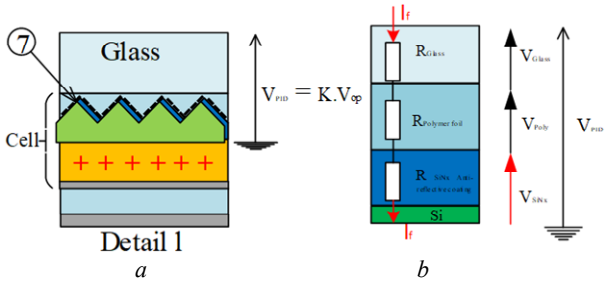

a *b*

Fig. 8. Cross-sectional modeling of a PV module

The voltage across the SiNx layer can be estimated using the model shown in Fig. 8,*b*

$$V_{SiNx} = \frac{R_{SiNx}}{R_{SiN\,x} + R_{Poly} + R_{Glass}} V_{PID}, \qquad (10)$$

where V_{PID} is the voltage between the front glass of the module and the surface of the encapsulated silicon cells; V_{SiNx} is the voltage between layer SiNx; R_{SiNx}, R_{Poly}, R_{Glass} are respectively the resistances of SiNx layer, EVA layer and glass.

The glass or polymer layers have high resistivity, while the silicon nitride (SiNx) layers are highly conductive. This combination helps resist PID by reducing the voltage across the SiNx film. The encapsulation material surrounding the PV cells provides thermal stability, protection against moisture, UV degradation resistance, and electrical insulation for the module components. A higher overall resistivity leads to a lower leakage current for a given potential difference, which reduces the accumulation of voltage on the surface of the solar cells, thus mitigating the effects of PID. The variation in resistance between the PV cell and the module frame is a critical indicator of PID in a PV system. This measurement helps assess the module's integrity and identify anomalies related to insulation.

PID modeling. Researchers have studied how PID affects PV modules at different voltages (750 V, 500 V, 250 V) under constant conditions of 70 °C temperature and 100 g/m³ humidity. They found that the degradation over time follows an exponential pattern. At first, the degradation happens quickly, but the rate slows down over time. Eventually, the PID degradation rate becomes very small or almost zero. This behavior can be described as:

$$PID(t) = PID_{\infty}[1 - e^{-t/\tau}], \qquad (11)$$

where $PID_{\infty} = \lim_{t\to\infty} PID$ is the maximum degradation level of a PV module caused by *PID* at infinite time; t is the PID stress duration; τ is the time constant.

PID_{∞} increases as the applied voltage rises, for instance, at 250 V, 500 V and 750 V. The value of τ indicates the rate at which *PID* reaches its limit. It depends on the PID resistance properties of the PV module materials and the environmental conditions. PV module with high PID resistance will have a higher τ, requiring more time to reach PID_{∞}. Conversely, a PV module with low *PID* resistance will have a lower τ, reaching PID_{∞} in a shorter time. Therefore, we can define:

$$R_{sh,\deg}(t) = R_{sh0} e^{(-t/\tau)}, \qquad (12)$$

where $R_{sh,\deg}(t)$ is the degraded shunt resistance value corresponding to PID_{∞}

Through extensive experiments and testing, a model was developed to understand the impact of various parameters on PID. It was observed that the leakage current increases proportionally to the square of the operating voltage (panel-to-ground voltage). Similarly, the leakage current is also proportional to the square of the panel's lifespan and the square of the relative humidity. Additionally, the leakage current follows an Arrhenius relationship, with activation energy of 0.94 eV. The shunt resistance in the equivalent circuit of the PV cell models the leakage current. Its variation is fitted to the following [14]:

$$R_{sh,\deg}(t) = \frac{1}{7\cdot 10^{-6} V_{op}^2 R_H^2 \exp\left(-\frac{90700}{RT_{avg}}\right) t^2}, \qquad (13)$$

where V_{op} is the operating voltage of the panel (panel-to-ground voltage); R_H is the relative humidity; R is the gas constant; T_{avg} is the average temperature; t is the time.

The degraded shunt resistance also depends on the position of the PV cell relative to the metal frame of the PV module. When the cell is closer to the frame, the degradation rate caused by PID becomes more severe. Similarly, cells located in the corners experience an even higher intensity of degradation. To do this, a factor that characterizes this condition is added to (7), as shown in Fig. 9.

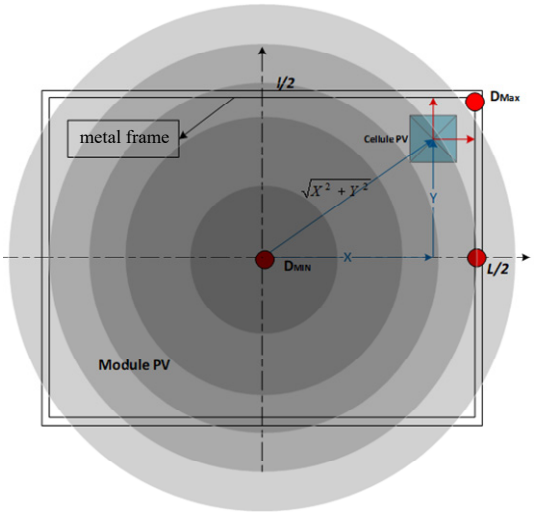

Fig. 9.The distribution of the parallel resistance of a PV cell based on its position within the PV module

At the corner of the PV module, degradation by the PID process is maximal, while at the center of the PV module, degradation is minimal. We can define a function whose lowest value is at the center of the panel and the highest value is near the edges. Therefore, the following equation determines a normalization coefficient which represents the position of PV cell encapsulated in the PV module relative to its center

$$r_{(n,m)} = \frac{\sqrt{X^2 + Y^2}}{\sqrt{(L/2)^2 + (l/2)^2}}; \qquad (14)$$

$$R_{sh,\deg(n,m)} = R_{sh,\deg} \cdot r_{(n,m)}, \qquad (15)$$

where $R_{sh,\deg(n,m)}$ is the degraded shunt resistance in relation to their position within the encapsulation; $r_{(n,m)}$ is the normalization coefficient; X, Y are the horizontal and vertical positions of the center of the PV module, respectively; L, l are the length and width of the PV module, respectively.

Experiments. All measurements are carried out under stable weather conditions, with uniform illumination, consistent temperature, and identical tilt angles for both modules. This method ensures measurement reliability by reducing the impact of environmental variables. The experimental parameters, such as irradiation, humidity (both high and low), air temperature and panel temperature were carefully controlled throughout the tests. The average irradiance was estimated at 800 W/m^2, and the ambient temperature was approximately 32 °C during the tests, which were conducted around noon from September 25th to 30th, a period characterized by hot and sunny days. Regarding

humidity, module 1 was exposed to both dry and humid environments, with a relative humidity exceeding 85 %. This exposure was essential to analyze and compare the behavior of the two PV modules subjected to outdoor rooftop conditions for 5 years without being operational. Both modules experienced similar climatic and environmental conditions during this period. These field testing conditions differ significantly from laboratory tests conducted in accordance with the IEC 62804 standard.

We examined two identical PV modules (Module 1 and Module 2) from the same brand, exposed to the same climatic conditions (Fig. 10). For this reason, under both dry and humid conditions, we used an insulation tester Megger 5 kV to practically demonstrate how the voltage of a PV string (V_{op}) affects the insulation resistance and triggers the PID degradation process in a PV module. Initially, both modules exhibited similar *I-V* behavior under both dry and humid conditions. We applied a DC voltage of up to 1 kV between the positive terminal and carefully selected points on the metal frame and glass surface of the front of the PV module to measure the corresponding insulation resistance. This test helps determine whether the PV module maintains adequate insulation or shows signs of degradation that could impact its long-term performance. Moreover, while ensuring similar climatic conditions, we conducted voltage and current measurements at several operating points of both Module 1 and Module 2. This allowed us to plot their *I-V* characteristic curves, providing an overview of their performance. It also illustrated how the voltage in a PV string affects insulation resistance and triggers the PID process.

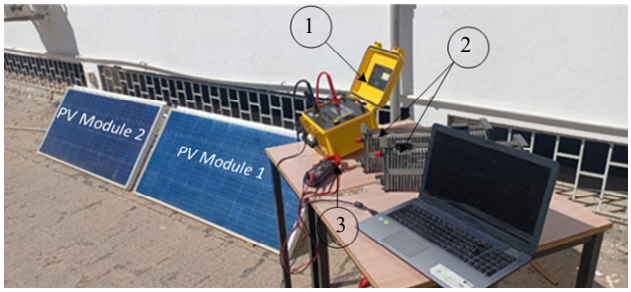

Fig. 10. An experimental test bench with two PV modules: 1 – insulation tester; 2 – two variable resistors, each rated at 10 A; 3 – ammeters and voltmeters

Measurements and results. The insulation resistance of a PV module is significantly influenced by the applied test voltage. For this reason, under dry or humid conditions, we applied different levels of DC voltage between the positive terminal of the PV module and its metal frame, while accurately measuring the corresponding insulation resistance for each voltage level, as shown in Fig. 11, 12. The purpose of this test is to simulate the module's real operating conditions by subjecting it to voltages generated by the Megger, similar to those it encounters during its actual operation in a PV string.

The insulation resistance of the module (Table 2) indicates that an increase in the test voltage leads to a decrease in the insulation resistance. Furthermore, a humid environment also causes a significant reduction in this insulation resistance compared to the value measured in a dry environment.

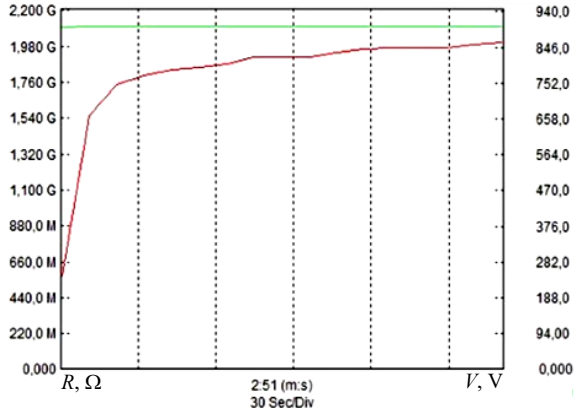

Fig. 11. Insulation resistance of the module under of 1 kV DC in a damp environment

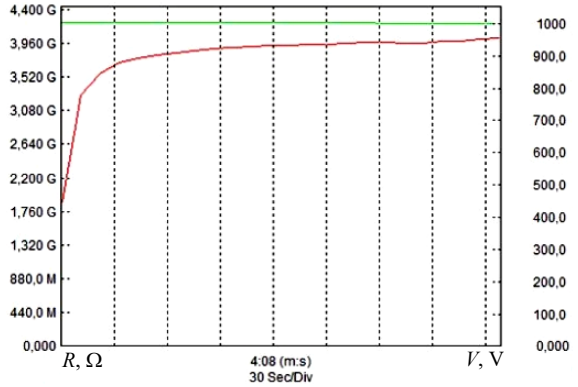

Fig. 12. Insulation resistance of the module under of 1 kV DC in a dry environment

Table 2

Isolation resistance values for dry and damp conditions

	Insulation resistance, GΩ	
Applied voltage, V	Dry environment	Damp environment
500	4.24	2.47
700	4.17	2.19
900	4.13	1.98
1000	3.96	1.76

The degradation rate *D* is:

$$D = \left(1 - \frac{P_{M1\max}}{P_{M2\max}}\right) \cdot 100\% , \qquad (14)$$

where $P_{M1\max}$, $P_{M2\max}$ are the maximum power generated by Module 1 and Module 2, respectively.

The theoretical maximum power of the module shows degradation, dropping from 142 W before testing to 123 W after dry condition tests, representing a decrease of 11 W or a degradation rate of 7.7 %. Conversely, after wet condition tests, the power reaches 123 W, reflecting a drop of 19 W, equivalent to a degradation rate of 13 %. This reduction in theoretical maximum power is attributed to the decrease in short-circuit current (I_{sc}), as shown in Table 3.

Table 3

Values of V_{oc} and I_{sc} before and after dry and wet testing

	Not stressed module	Dry env. stressed module	Humid env. stressed module
V_{oc}, V	20.1	19.93	20.91
I_{sc}, A	7.07	6.58	5.91
$P_{\max}$, W	142.107	131.139	123.578

The increase in open-circuit voltage (V_{oc}) under wet conditions is due to the reduction in module temperature

caused by these testing conditions. It can be concluded in this section that the reduction in insulation resistance may increase the electric field within the SiNx layer, potentially causing polarization of this layer. Such polarization can interfere with current generation, leading to a loss of efficiency in the PV module due to PID.

The procedure for the insulation resistance test involves selecting specific measurement points on the module. Three points (no. 2, no. 3, no. 4) are chosen diagonally on the front glass surface, with a lengthwise spacing of 25.4 cm and a widthwise spacing of 11 cm (Fig. 13). Additionally, two points are identified on the aluminum frame: point no. 1 is located at the top-right corner of the frame, while point no. 5 is positioned at the center of the right vertical rail. Once these points are established, the resistance between the module's positive terminal and each of these points is measured. The measurements are conducted under a dry environment and a wet environment.

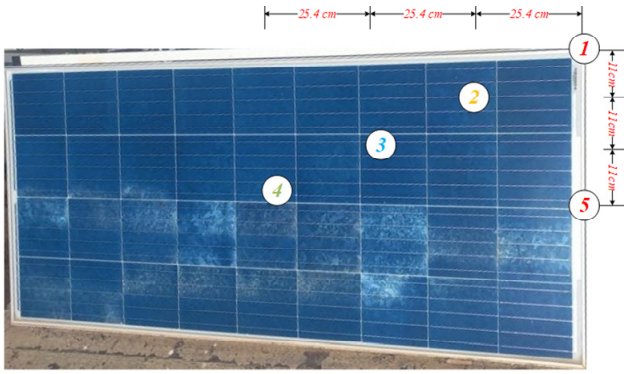

Fig. 13. Measurement points for insulation resistance test

The insulation resistance of the module, measured at different points on the glass and the frame, reveals that the resistance at the selected points on the frame is lower compared to that measured on the glass. The insulation resistance at the corner of the frame (point 1) is lower than at point 2, located in the middle of the frame's vertical rail. This indicates increased susceptibility to PID at this location. As one moves toward the center of the module, away from the frame, the insulation resistance increases, providing better protection against PID. It can be concluded that PV cells located at the corners of the module's frame are the most stressed and the first to experience the effects of PID.

Characteristics of the two modules and comparison of results. At this stage, Module 2 was chosen as the reference module, as it had not been exposed to the high voltages previously applied to Module 1. To determine the operating points of the PV module, a variable resistor was utilized. Under the same weather conditions, similar measurements were conducted simultaneously on Module 1.

By identification, R_{sh} represents the slope of the characteristic *I-V* curve of the module to the left of the maximum power point

$$I \approx I_{sc} - (V/R_{sh}). \quad (15)$$

In our case, R_{sh} refers to the specific value ($R_{sh} \approx 120\ \Omega$) that reflects the rate of change in current with respect to voltage before reaching the maximum power point (Fig. 14, 15).

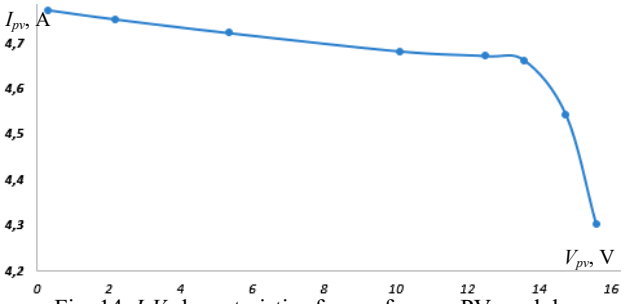

Fig. 14. *I-V* characteristics for a reference PV module

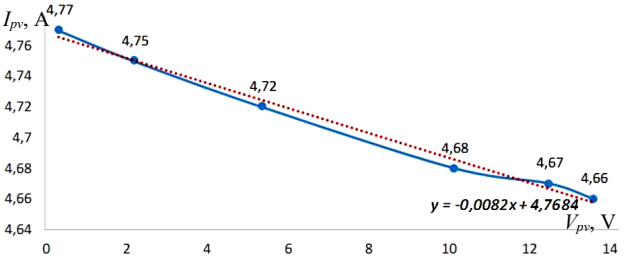

Fig. 15. R_{sh} represented by the inverse of the slope of the dashed line (unstressed module)

As shown in Fig. 16, 17, it is observed that the shunt resistance R_{sh} of the stressed Module 1 has been evaluated $R_{sh} \approx 90\ \Omega$ is lower than that of the reference Module 2. Since R_{sh} represents the resistance of the parallel paths through which current can leak when a voltage is applied, we can conclude that the R_{sh} parameter of Module 1 has been degraded due to the voltage levels applied during the tests. Additionally, our module, equipped with two bypass diodes (a 32-cell module), shows bends in the *I-V* curve, even under uniform lighting conditions. These irregularities point to the effect of PID on the module's behavior. The bypass diodes are designed to protect the cells from overloads and shading; however, the presence of these bends suggests that, despite uniform lighting, certain cells experience performance losses. This could be due to increased resistance at connection points or variations in conductivity caused by PID. This phenomenon highlights the importance of monitoring and assessing the integrity of PV modules, even when lighting conditions appear to be ideal.

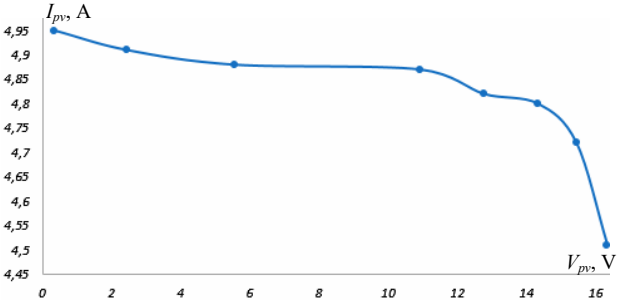

Fig. 16. *I-V* characteristics of PV stressed module

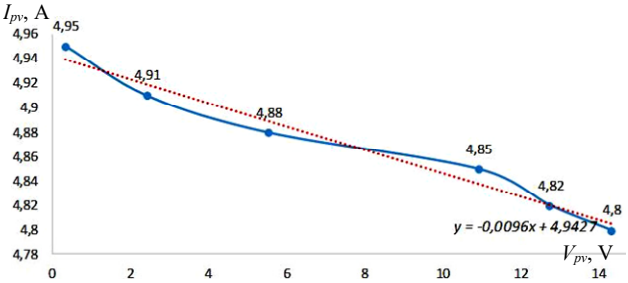

Fig. 17. R_{sh} represented by the inverse of the slope of the dashed line (stressed module)

Discussion. The test results conducted on the PV modules reveal several key aspects related to their performance and lifespan. The anomalies observed in the *I-V* characteristic curves, even under uniform illumination, suggest that PID negatively impacts the functioning of the cells. This implies that certain cells may be less efficient, leading to a reduction in the current generated. By comparing the values of R_{sh} between the reference module (Module 2) and the stressed module (Module 1), it is evident that R_{sh} in Module 1 is lower. This indicates that the parallel paths through which current can flow are compromised, which can impair the efficiency and reliability of the module. This degradation appears to be correlated with the voltages applied during the tests, emphasizing the importance of careful voltage management to maintain the performance of PV modules. The bypass diodes integrated into the module are designed to protect the cells from overheating and shading. However, the anomalies in the *I-V* curve could suggest that these diodes activate at certain times to compensate for current losses caused by PID. This raises questions about the potential for optimizing module design to better address these challenges. The results indicate that PID can have long-lasting effects on the reliability and efficiency of PV modules. Therefore, it is essential to regularly monitor their performance, with a particular focus on shunt resistance and *I-V* characteristics, in order to anticipate and address degradation issues. To reduce the impact of PID, it is recommended to choose high-quality materials, design optimized circuits, and install monitoring systems for early detection of anomalies. Additionally, a thorough evaluation of operating conditions, including voltage levels, is crucial to ensure optimal performance of PV modules.

Conclusions. This study offers a comprehensive evaluation of the performance of two identical PV modules under strictly controlled conditions, including irradiation, humidity (both high and low), air temperature, and panel temperature. The tests were conducted with an average irradiance of 800 W/m^2 and an ambient temperature of approximately 32 °C, around noon between September 25th and 30th, during hot and sunny days. By maintaining uniform illumination and stable temperature, we were able to isolate the effects of the applied voltage on the insulation resistance and electrical performance of the modules. The results indicate that an increase in test voltage leads to a decrease in insulation resistance, with a more pronounced reduction in a humid environment. Also significant decrease in the shunt resistance of the stressed module, from 120 Ω to 90 Ω, compared to the identical non-stressed module. This highlights the modules' susceptibility to potential-induced degradation, which could have significant implications for their longevity and efficiency. The analysis of the various measurement points on the modules revealed that the areas located at the corners of the frame are the most vulnerable, exhibiting lower insulation resistance values. This suggests that special attention should be given to these areas during the design and installation of PV modules. Regarding the *I-V* characteristics, the comparison between the reference module and the module subjected to high voltages showed clear signs of degradation, particularly in terms of shunt resistance. The irregularities in the *I-V* curve of the stressed module emphasize potential performance losses, even under uniform illumination. In conclusion, this study highlights the importance of regular monitoring of PV installations and continuous performance evaluation. To ensure long-term efficiency of PV systems, it is essential to explore solutions to mitigate the effects of potential-induced degradation and establish preventive maintenance protocols. Future research could focus on innovations in design and materials to minimize the vulnerability of modules to voltage-related degradation.

Conflict of interest. The authors declare that they have no conflicts of interest.

REFERENCES

1. *World Energy Outlook 2024*. International Energy Agency Publ., 2024, 398 p. Available at: https://iea.blob.core.windows.net/assets/140a0470-5b90-4922-a0e9-838b3ac6918c/WorldEnergyOutlook2024.pdf (Accessed: 30 August 2024).

2. Wiatros-Motyka M., Jones D., Fulghum N. *Global Electricity Review 2024*. Ember Publ., 2024, 191 p. Available at: https://ember-energy.org/app/uploads/2024/05/Report-Global-Electricity-Review-2024.pdf (Accessed: 30 August 2024).

3. Lyu L., Fang L. A Study on E-C Translation of BP Statistical Review of World Energy 2022 from the Perspective of Schema Theory. *Journal of Linguistics and Communication Studies*, 2023, vol. 2, no. 1, pp. 10-14. doi: https://doi.org/10.56397/JLCS.2023.03.02.

4. Fawzy S., Osman A.I., Doran J., Rooney D.W. Strategies for mitigation of climate change: a review. *Environmental Chemistry Letters*, 2020, vol. 18, no. 6, pp. 2069-2094. doi: https://doi.org/10.1007/s10311-020-01059-w.

5. Crippa M., Guizzardi D., Muntean M., Schaaf E., Solazzo E., Monforti-Ferrario F., Olivier J.G.J., Vignati E. *Fossil CO_2 emissions of all world countries - 2020 report*. Publ. Office of the EU, Luxembourg, 2020. 244 p. doi: https://doi.org/10.2760/143674.

6. Rossi R., Schmela M. *Global market outlook for solar power 2019–2023*. Solar Power Europe, Brussels, Belgium, Tech. Rep., 2019. Available at: https://www.solarpowereurope.org/insights/webinars/eu-market-outlook-solar-power-2019-2023 (Accessed: 30 August 2024).

7. Azizi A., Logerais P.-O., Omeiri A., Amiar A., Charki A., Riou O., Delaleux F., Durastanti J.-F. Impact of the aging of a photovoltaic module on the performance of a grid-connected system. *Solar Energy*, 2018, vol. 174, pp. 445-454. doi: https://doi.org/10.1016/j.solener.2018.09.022.

8. Bouaichi A., Alami Merrouni A., Hajjaj C., Messaoudi C., Ghennioui A., Benlarabi A., Ikken B., El Amrani A., Zitouni H. In-situ evaluation of the early PV module degradation of various technologies under harsh climatic conditions: The case of Morocco. *Renewable Energy*, 2019, vol. 143, pp. 1500-1518. doi: https://doi.org/10.1016/j.renene.2019.05.091.

9. Kim J., Rabelo M., Padi S.P., Yousuf H., Cho E.-C., Yi J. A Review of the Degradation of Photovoltaic Modules for Life Expectancy. *Energies*, 2021, vol. 14, no. 14, art. no. 4278. doi: https://doi.org/10.3390/en14144278.

10. Jordan D.C., Kurtz S.R. Photovoltaic Degradation Rates – an Analytical Review. *Progress in Photovoltaics: Research and Applications*, 2013, vol. 21, no. 1, pp. 12-29. doi: https://doi.org/10.1002/pip.1182.

11. Peshek T.J., Fada J.S., Martin I.T. Degradation processes in photovoltaic cells. *Durability and Reliability of Polymers and Other Materials in Photovoltaic Modules*, 2019, pp. 97-118. doi: https://doi.org/10.1016/B978-0-12-811545-9.00004-5.

12. Golive Y.R., Zachariah S., Dubey R., Chattopadhyay S., Bhaduri S., Singh H.K., Bora B., Kumar S., Tripathi A.K.,

Kottantharayil A., Vasi J., Shiradkar N. Analysis of Field Degradation Rates Observed in All-India Survey of Photovoltaic Module Reliability 2018. *IEEE Journal of Photovoltaics*, 2020, vol. 10, no. 2, pp. 560-567. doi: https://doi.org/10.1109/JPHOTOV.2019.2954777.

13. Buerhop C., Pickel T., Patel T., Fecher F.W., Zetzmann C., Camus C., Hauch J., Brabec C.J. Analysis of inhomogeneous local distribution of potential induced degradation at a rooftop photovoltaic installation. *IET Renewable Power Generation*, 2017, vol. 11, no. 10, pp. 1253-1260. doi: https://doi.org/10.1049/iet-rpg.2017.0105.

14. Nehme B.F., Akiki T.K., Naamane A., M'Sirdi N.K. Real-Time Thermoelectrical Model of PV Panels for Degradation Assessment. *IEEE Journal of Photovoltaics*, 2017, vol. 7, no. 5, pp. 1362-1375. doi: https://doi.org/10.1109/JPHOTOV.2017.2711430.

15. Ahmad J., Ciocia A., Fichera S., Murtaza A.F., Spertino F. Detection of Typical Defects in Silicon Photovoltaic Modules and Application for Plants with Distributed MPPT Configuration. *Energies*, 2019, vol. 12, no. 23, art. no. 4547. doi: https://doi.org/10.3390/en12234547.

16. Haque A., Bharath K.V.S., Khan M.A., Khan I., Jaffery Z.A. Fault diagnosis of Photovoltaic Modules. *Energy Science & Engineering*, 2019, vol. 7, no. 3, pp. 622-644. doi: https://doi.org/10.1002/ese3.255.

17. Kwembur I.M., Crozier McCleland J.L., Van Dyk E.E., Vorster F.J. Detection of Potential Induced Degradation in mono and multi-crystalline silicon photovoltaic modules. *Physica B: Condensed Matter*, 2020, vol. 581, art. no. 411938. doi: https://doi.org/10.1016/j.physb.2019.411938.

18. Luo W., Khoo Y.S., Hacke P., Naumann V., Lausch D., Harvey S.P., Singh J.P., Chai J., Wang Y., Aberle A.G., Ramakrishna S. Potential-induced degradation in photovoltaic modules: a critical review. *Energy & Environmental Science*, 2017, vol. 10, no. 1, pp. 43-68. doi: https://doi.org/10.1039/C6EE02271E.

19. Rahman M.M., Khan I., Alameh K. Potential measurement techniques for photovoltaic module failure diagnosis: A review. *Renewable and Sustainable Energy Reviews*, 2021, vol. 151, art. no. 111532. doi: https://doi.org/10.1016/j.rser.2021.111532.

20. Lee S., Bae S., Park S.J., Gwak J., Yun J., Kang Y., Kim D., Eo Y.-J., Lee H.-S. Characterization of Potential-Induced Degradation and Recovery in CIGS Solar Cells. *Energies*, 2021, vol. 14, no. 15, art. no. 4628. doi: https://doi.org/10.3390/en14154628.

21. Roy S., Kumar S., Gupta R. Investigation and analysis of finger breakages in commercial crystalline silicon photovoltaic modules under standard thermal cycling test. *Engineering Failure Analysis*, 2019, vol. 101, pp. 309-319. doi: https://doi.org/10.1016/j.engfailanal.2019.03.031.

22. Dhimish M., Badran G. Recovery of Photovoltaic Potential-Induced Degradation Utilizing Automatic Indirect Voltage Source. *IEEE Transactions on Instrumentation and Measurement*, 2022, vol. 71, pp. 1-9. doi: https://doi.org/10.1109/TIM.2021.3134328.

23. Carolus J., Tsanakas J.A., van der Heide A., Voroshazi E., De Ceuninck W., Daenen M. Physics of potential-induced degradation in bifacial p-PERC solar cells. *Solar Energy Materials and Solar Cells*, 2019, vol. 200, art. no. 109950. doi: https://doi.org/10.1016/j.solmat.2019.109950.

24. Wang H., Cheng X., Yang H., He W., Chen Z., Xu L., Song D. Potential-induced degradation: Recombination behavior, temperature coefficients and mismatch losses in crystalline silicon photovoltaic power plant. *Solar Energy*, 2019, vol. 188, pp. 258-264. doi: https://doi.org/10.1016/j.solener.2019.06.023.

25. Srinivasan A., Devakirubakaran S., Meenakshi Sundaram B. Mitigation of mismatch losses in solar PV system – Two-step reconfiguration approach. *Solar Energy*, 2020, vol. 206, pp. 640-654. doi: https://doi.org/10.1016/j.solener.2020.06.004.

26. Zied K., Hechmi K., Hedi M.M., Abderrahmen Z. Efficiency of different control algorithms for a PV panel. *2022 IEEE International Conference on Electrical Sciences and Technologies in Maghreb (CISTEM)*, 2022, pp. 1-6. doi: https://doi.org/10.1109/CISTEM55808.2022.10043961.

27. Khammassi Z., Chrouta J., Moulehi M.H., Zaafouri A. Comparative study of different types of PV plant grounding on the Potential Induced Degradation. *2023 9th International Conference on Control, Decision and Information Technologies (CoDIT)*, 2023, pp. 2677-2682. doi: https://doi.org/10.1109/CoDIT58514.2023.10284498.

28. Shweta R., Sivagnanam S., Kumar K.A. Fault detection and monitoring of solar photovoltaic panels using internet of things technology with fuzzy logic controller. *Electrical Engineering & Electromechanics*, 2022, no. 6, pp. 67-74. doi: https://doi.org/10.20998/2074-272X.2022.6.10.

29. Latreche S., Khenfer A., Khemliche M. Sensors placement for the faults detection and isolation based on bridge linked configuration of photovoltaic array. *Electrical Engineering & Electromechanics*, 2022, no. 5, pp. 41-46. doi: https://doi.org/10.20998/2074-272X.2022.5.07.

30. Lahiouel Y., Latreche S., Khemliche M., Boulemzaoud L. Photovoltaic fault diagnosis algorithm using fuzzy logic controller based on calculating distortion ratio of values. *Electrical Engineering & Electromechanics*, 2023, no. 4, pp. 40-46. doi: https://doi.org/10.20998/2074-272X.2023.4.06.

Received 01.12.2024
Accepted 25.01.2025
Published 02.07.2025

Z. Khammassi [1]*, PhD,*
H. Khaterchi [1]*, PhD,*
A. Zaafouri [1]*, Professor of Electrical Engineering,*
[1] University of Tunis,
Higher National Engineering School of Tunis,
Industrial Systems Engineering and Renewable Energies
Research Laboratory, Tunisia,
e-mail: ziedkhammassi@yahoo.fr (Corresponding Author);
hechmi.khaterchi@uvt.tn; rhaiem.zaafouri@ensit.rnu.tn

How to cite this article:
Khammassi Z., Khaterchi H., Zaafouri A. Experimental analysis of the effects of potential-induced degradation on photovoltaic module performance parameters. *Electrical Engineering & Electromechanics*, 2025, no. 4, pp. 35-43. doi: https://doi.org/10.20998/2074-272X.2025.4.05